



1 **Recent acceleration of Denman Glacier (1972-2017), East Antarctica, driven by**  
2 **grounding line retreat and changes in ice tongue configuration.**

3

4 Bertie W.J. Miles<sup>1\*</sup>, Jim R. Jordan<sup>2</sup>, Chris R. Stokes<sup>1</sup>, Stewart S.R. Jamieson<sup>1</sup>, G. Hilmar  
5 Gudmundsson<sup>2</sup>, Adrian Jenkins<sup>2</sup>

6 <sup>1</sup>Department of Geography, Durham University, Durham, DH1 3LE, UK

7 <sup>2</sup>Department of Geography and Environmental Sciences, Northumbria University, Newcastle upon Tyne, NE1  
8 8ST, UK

9 \*Correspondence to: a.w.j.miles@durham.ac.uk

10

11 **Abstract:** Denman Glacier is one of the largest in East Antarctica, with a catchment that  
12 contains an ice volume equivalent to 1.5 m of global sea-level and which sits in the Aurora  
13 Subglacial Basin (ASB). Geological evidence of this basin's sensitivity to past warm periods,  
14 combined with recent observations showing that Denman's ice speed is accelerating, and its  
15 grounding line is retreating along a retrograde slope, have raised the prospect that it could  
16 contribute to near-future sea-level rise. In this study, we produce the first long-term (~ 50 years)  
17 record of past glacier behaviour (ice flow speed, ice tongue structure, and calving) and combine  
18 these observations with numerical modelling to explore the likely drivers of its recent change.  
19 We find a spatially widespread acceleration of the Denman system since the 1970s across both  
20 its grounded ( $17 \pm 4\%$  acceleration; 1972-2017) and floating portions ( $36 \pm 5\%$  acceleration;  
21 1972-2017). Our numerical modelling experiments show that a combination of grounding line  
22 retreat, ice tongue thinning and the unpinning of Denman's ice tongue from a pinning point  
23 following its last major calving event are required to simulate an acceleration comparable with  
24 observations. Given its bed topography and the geological evidence that Denman Glacier has  
25 retreated substantially in the past, its recent grounding line retreat and ice flow acceleration  
26 suggest that it could be poised to make a significant contribution to sea level over the coming  
27 century.

28

29 **1. Introduction**

30 Over the past two decades, outlet glaciers along the coastline of Wilkes Land, East Antarctica,  
31 have been thinning (Pritchard et al., 2009; Flament and Remy, 2012; Helm et al., 2014;



32 Schröder et al., 2018), losing mass (King et al., 2012; Gardner et al., 2018; Shen et al., 2018;  
33 Rignot et al., 2019) and retreating (Miles et al., 2013; Miles et al., 2016). This has raised  
34 concerns about the future stability of some major outlet glaciers that primarily drain the Aurora  
35 Subglacial Basin (ASB), particularly Totten, Denman, Moscow University and Vanderford  
36 Glaciers (Fig. 1). This is because their present day grounding lines are close to deep retrograde  
37 slopes (Morlighem et al., 2020), meaning there is clear potential for marine ice sheet instability  
38 and future rapid mass loss (Weertman, 1974; Schoof, 2007), unless ice shelves provide a  
39 sufficient buttressing effect (Gudmundsson, 2013). Geological evidence suggests that there  
40 may have been substantial retreat of the ice margin in the ASB during the warm interglacials  
41 of the Pliocene (Williams et al., 2010; Young et al., 2011; Aitken et al., 2016; Scherer et al.,  
42 2016), which potentially resulted in global mean sea level contributions of up to 2 m from the  
43 ASB (Aitken et al., 2016). This is important because these warm periods of the Pliocene may  
44 represent our best analogue for climate by the middle of this century under unmitigated  
45 emission trajectories (Burke et al., 2018). Indeed, numerical models now predict future sea  
46 level contributions from the outlet glaciers which drain the ASB over the coming decades to  
47 centuries (Golledge et al., 2015; Ritz et al., 2015; DeConto and Pollard, 2016), but large  
48 uncertainties exist over the magnitude and rates of any future sea level contributions.

49 At present, most studies in Wilkes Land have focused on Totten Glacier which is losing mass  
50 (Li et al., 2016; Mohajerani et al., 2019) in association with grounding line retreat (Li et al.,  
51 2015). This has been attributed to wind-forced warm Modified Circumpolar Deep Water  
52 accessing the cavity below Totten Ice Shelf (Greenbaum et al., 2015; Rintoul et al., 2016;  
53 Greene et al., 2017). However, given our most recent understanding of bedrock topography in  
54 Wilkes Land, Denman Glacier provides the most direct pathway to the deep interior of the ASB  
55 (Gasson et al., 2015; Brancato et al., 2020; Morlighem et al., 2020). Moreover, a recent mass  
56 balance estimate (Rignot et al., 2019) has shown that, between 1979 and 2017, Denman  
57 Glacier's catchment may have lost an amount of ice (190 Gt) broadly comparable with Totten  
58 Glacier (236 Gt). There have also been several reports of inland thinning of Denman's fast-  
59 flowing trunk (Flament and Remy, 2012; Helm et al., 2014; Young et al., 2015; Schröder et  
60 al., 2018) and its grounding line has retreated over the past 20 years (Brancato et al., 2020).  
61 However, unlike Totten and other large glaciers which drain marine basins in Antarctica, there  
62 has been no detailed study analysing any changes in its calving cycle, velocity or ice tongue  
63 structure. This study reports on a range of remote sensing observations from 1962 to 2018 and  
64 then brings these observations together with numerical modelling to explore the possible



65 drivers of Denman's long-term behaviour. The following section outlines the methods (section  
66 2) used to generate the remote sensing observations (section 3) and we then outline the  
67 numerical modelling experiments (section 4) that were motivated by these observations,  
68 followed by the discussion (section 5).

69

## 70 **2. Methods**

### 71 *2.1 Ice front and calving cycle reconstruction*

72 We use a combination of imagery from the ARGON (1962), Landsat-1 (1972-74), Landsat 4-  
73 5 (1989-1991), RADARSAT (1997) and Landsat 7-8 (2000-2018) satellites to create a time  
74 series of ice-front position change from 1962-2018. Suitable cloud-free Landsat imagery was  
75 first selected using the Google Earth Engine Digitisation Tool (Lea, 2018). Changes in ice-  
76 front position were calculated using the box method, which uses an open ended polygon to take  
77 into account any uneven changes along the ice-front (Moon and Joughin, 2008). To supplement  
78 the large gap in the satellite archive between 1974 and 1989 we use the RESURS KATE-200  
79 space-acquired photography from September 1984. This imagery is hosted by the Australian  
80 Antarctic Data Centre, and whilst we could not access the full resolution image, the preview  
81 image was sufficient to determine the approximate location of the ice-front and confirm that a  
82 major calving event took place shortly before the image was acquired (Fig. S1).

83

### 84 *2.2 Velocity*

85 Maps of glacier velocity between 1972 and 2002 were created using the COSI-Corr (CO-  
86 registration of Optically Sensed Images and Correlation) feature-tracking software (Leprince  
87 et al., 2007; Scherler et al., 2008). This requires pairs of cloud-free images where surface  
88 features can be identified in both images. We found three suitable image pairs from the older  
89 satellite data: Nov 1972 – Feb 1974, Feb 1989 – Nov 1989, and Nov 2001 – Dec 2002. We  
90 used a window size of 128 x 128 pixels, before projecting velocities onto a WGS 84 grid at a  
91 pixel spacing of 1 km.

92 To reduce noise, we removed all pixels where ice speed was greater than  $\pm 50\%$  the MEaSUREs  
93 ice velocity product (Rignot et al., 2011b), and all pixels where velocity was  $< 250 \text{ m yr}^{-1}$ . Errors  
94 are estimated as the sum of the co-registration error (estimated at 1 pixel) and the error in



95 surface displacement (estimated at 0.5 pixels). This resulted in total errors ranging from 20 to  
96 73 m yr<sup>-1</sup>. Annual estimates of ice speed between 2005-2006 and 2016-2017 were taken from  
97 the annual MEaSURES mosaics (Mouginot et al., 2017). These products are available at a 1  
98 km spatial resolution and are created from the stacking of multiple velocity fields from a variety  
99 of sensors between July and June in the following year. To produce the ice speed time-series,  
100 we extracted the mean value of all pixels within a defined box 10 km behind Denman's  
101 grounding line (see Fig. 3). To eliminate any potential bias from missing pixels, we placed  
102 boxes in locations where all pixels were present at each time step.

103 We also estimated changes in the rate of ice-front advance between 1962 and 2018. This is  
104 possible because inspection of the imagery reveals that there has been only one major calving  
105 event at Denman during this time period because the shape of its ice front remained largely  
106 unchanged throughout the observation period. Similar methods have been used elsewhere on  
107 ice shelves which have stable ice fronts e.g. Cook East Ice Shelf (Miles et al., 2018). This has  
108 the benefit of acting as an independent cross-check on velocities close to the front of the ice  
109 tongue that were derived from feature tracking. Whilst the accuracy of velocity fields produced  
110 by modern satellites (e.g. Sentinel-1; Landsat-8) have been established, the accuracy of velocity  
111 fields produced by earlier, coarser resolution satellite images (e.g. Landsat-1) are largely  
112 untested. The ice-front advance rate was calculated by dividing ice-front position change by  
113 the number of days between image pairs. Errors are associated with co-registration (1 pixel)  
114 and manual mapping of the ice-front (0.5 pixels), resulting in errors ranging from 6 to 73 m yr<sup>-1</sup>.  
115 The general pattern of ice-front advance rates through time is in close agreement with feature  
116 tracking-derived changes in velocity over the same time period.

117

### 118 **3. Results**

#### 119 ***3.1 Ice tongue calving cycles and structure***

120 Throughout our observational record (1962 - 2018) Denman Glacier underwent only one major  
121 calving event, in 1984, which resulted in the formation of a large 54 km long (1,800 km<sup>2</sup>)  
122 tabular iceberg (Fig. 2a-c). Since this calving event in 1984 the ice-front has re-advanced 60  
123 km and there have been no further major calving events (Fig. 2a, b), as indicated by minimal  
124 changes to the geometry of its 35 km wide ice front. As of November 2018, Denman Glacier's  
125 ice-front was approximately 6 km further advanced than its estimated calving front position  
126 immediately prior to the major calving event in 1984 (Fig. 2a, b). However, given the absence



127 of any significant rifting or structural damage, a calving event in the next few years is unlikely.  
128 This suggests the next calving event at Denman will take place from a substantially more  
129 advanced position (>10 km) than its last observed event in 1984.

130 Following the production of the large tabular iceberg from Denman Glacier in 1984, it drifted  
131 ~60 km northwards before grounding on the sea floor (Fig. 2c), and remained near stationary  
132 for 20 years before breaking up and dispersing in 2004. Historical observations of sporadic  
133 appearances of a large tabular iceberg in this location in 1840 (Cassin and Wilkes, 1858) and  
134 1914 (Mawson, 1915), but not in 1931 (Mawson, 1932), suggest that these low-frequency,  
135 high-magnitude calving events are typical of the long-term behaviour of Denman Glacier. In  
136 1962, our observations indicate a similar large tabular iceberg was present at the same location  
137 (Fig. 2d) and, through extrapolation of the ice-front advance rate between 1962 and 1974 (Fig.  
138 2a), we estimate that this iceberg was produced at some point in the mid-1940s. However, the  
139 iceberg observed in 1962 (~2,700 km<sup>2</sup>) was approximately 50% larger in area than the iceberg  
140 produced in 1984 (~1,700 km<sup>2</sup>), and 35% longer (73 km versus 54 km). Thus, whilst Denman's  
141 next calving event will take place from a substantially more advanced position than it did in  
142 1984, it may not be unusual in the context of the longer-term behaviour of Denman Glacier  
143 (Fig. 2a).

144 There are clear differences in the structure of Denman Glacier between successive calving  
145 cycles. In all available satellite imagery between the 1940s and the calving event in 1984 (e.g.  
146 1962, 1972 and 1974) an increasing number of rifts (labelled R1 to R7) were observed on its  
147 ice tongue throughout this time (Fig. 2e). The rifts periodically form ~10 km inland of  
148 Chugunov Island (Fig. 2e), on the western section of the ice tongue, before being advected  
149 down-flow. An analysis of the rifting pattern in 1974 and the iceberg formed in 1984 indicates  
150 that the iceberg calved from R7 (Fig. 2c, e). In contrast, on both the grounded iceberg observed  
151 in 1962 (Fig. 2d), which likely calved in the 1940s, and on the present day calving cycle (1984-  
152 present; Fig. 3f), similar rifting patterns are not observed.

153

### 154 **3.2 Ice Speed**

155 We observed widespread increases in ice speed across the entire Denman system between  
156 1972-74 and 2016-17, with accelerations of  $19 \pm 5\%$  up to 50 km inland of the grounding line  
157 along the main trunk of the glacier (Fig. 3a). Specifically, at box *D*, 10 km inland of the  
158 grounding line, ice flow speed increased by  $17 \pm 4\%$  between 1972-74 and 2016-17 (Fig. 3c).



159 The largest rates of acceleration at box *D* took place between 1972-74 and 1989 when there  
160 was a speed-up of  $11 \pm 5\%$ . Between 1989 and 2016-17 there was a comparatively slower  
161 acceleration of  $3 \pm 2\%$  (Fig. 3c). The advance rate of the ice-front followed a similar pattern,  
162 but accelerated at a much greater rate. The ice-front advance rate increased by  $26 \pm 5\%$  between  
163 1972-74 and 1989, whilst increasing at a slower rate between 1989 and 2018 ( $9 \pm 1\%$ ; Fig. 3b).  
164 At box *S* on the neighbouring Scott Glacier, we observed a  $17 \pm 10\%$  decrease in velocity  
165 between 1972-74 and 2016-17 (Fig. 3d). Similar decreases in ice flow speed are also observed  
166 near the shear margin between Shackleton Ice Shelf and Denman Glacier (Fig. 3a, e). The net  
167 result of an increase in velocity at Denman Glacier and decreases in velocity either side at the  
168 Shackleton Ice Shelf and Scott Glacier is a steepening of the velocity gradient at the shear  
169 margins (Fig. 3e). Ice speed profiles across Denman Glacier also indicate lateral migration of  
170 the shear margins of  $\sim 5$  km in both the east and west directions through time (Fig. 3e).

171

### 172 **3.3 Lateral migration of Denman's ice tongue**

173 A comparison of satellite imagery between 1974 and 2002, when Denman's ice-front was in a  
174 similar location (e.g. Fig. 4b, c), reveals a lateral migration of its ice tongue and a change in  
175 the characteristics of the shear margins. North of Chugunov Island, towards the ice-front, we  
176 observe a bending and westward migration of the ice tongue in 2002, compared to its 1974  
177 position (Fig. 4b, c). In 1974, the ice tongue was intensely shearing against Chugunov Island,  
178 as indicated by the heavily damaged shear margins (Fig. 4d). However, by 2002 the ice tongue  
179 made substantially less contact with Chugunov Island because this section of the ice tongue  
180 migrated westwards (Fig. 4d, e). South of Chugunov Island there was a greater divergence of  
181 flow between the Denman and Scott Glaciers in 2002 compared to 1974, resulting in a more  
182 damaged shear margin (Fig. 4d, e). On the western shear margin between Shackleton Ice Shelf  
183 and Denman's ice tongue there was no obvious change in structure between 1974 and 2002  
184 (Fig. 4f, g). However, velocity profiles in this region show an eastward migration of the fast  
185 flowing ice tongue (Fig. 3e).

186

## 187 **4. Numerical Modelling**

### 188 **4.1. Model Set-Up and Experimental Design**



189 To help assess the possible causes of the acceleration of Denman Glacier since 1972 and the  
190 importance of changes we observe on Denman's ice tongue, we conduct diagnostic numerical  
191 modelling experiments using the finite-element, ice dynamics model *Úa* (Gudmundsson et al,  
192 2012). *Úa* is used to solve the equations of the shallow-ice stream or 'shelfy-stream'  
193 approximation, (SSA, Cuffey & Paterson, 2010). Previously the model has been used to  
194 understand rates and patterns of grounding line migration, and glacier responses to ice shelf  
195 buttressing and ice shelf thickness (e.g. Reese et al., 2018; Hill et al., 2019; Gudmundsson et  
196 al., 2019), and has been involved in several model intercomparison experiments (e.g. Pattyn et  
197 al., 2008; 2012; Leverman et al., 2020).

198 Modelled ice velocities are calculated on a finite-element grid using a vertically-integrated  
199 form of the momentum equations. The model domain consists of 93,371 elements with  
200 horizontal dimensions ranging from 250 m near the grounding line to 10 km further inland.  
201 Zero flow conditions are applied along the inland boundaries, chosen to match zero flow  
202 contours from observations. Ice rheology is assumed to follow Glen's flow law, using stress  
203 exponent  $n=3$  and basal sliding is assumed to follow Weertman's sliding law, with its own  
204 stress exponent,  $m=3$ . Other modelling parameters related to ice rheology and basal conditions  
205 are the basal slipperiness,  $C$ , and the rate factor,  $A$ . We initialized the ice-flow model by  
206 changing both the ice rate factor  $A$  (Fig. S2b) and basal slipperiness  $C$  (Fig. S2c), using an  
207 inverse approach (Vogel, 2002), iterating until the surface velocities of the numerical model  
208 closely matched the 2009 measurements of ice flow (Fig. S2a).

209

#### 210 **4.2. Perturbation Experiments**

211 We start from a baseline set-up at a fixed point in time where both velocity and ice geometry  
212 are well-known. We chose 2009 for this baseline setup, because the calving front is in  
213 approximately the same position as in 1972 when our glacier observations start. We use the  
214 BedMachine (Morlighem et al., 2020) ice thickness, bathymetry and grounding line position  
215 and MEaSURES ice velocities for 2009 (Mouginot et al., 2017) as inputs. The baseline  
216 simulation is then perturbed to test its response to a series of potential drivers that may be  
217 responsible for the observed changes in ice geometry since the 1970s. Specifically, we apply  
218 observation-based perturbations to test Denman's response to ice shelf thinning (i), grounding  
219 line retreat (ii) and the unpinning of Denman's ice tongue from Chugunov Island (iii), which  
220 are detailed below:



221 i. To represent ice shelf thinning since 1972, we take the mean annual rate of ice-thickness  
222 change from the 1994–2012 ice-shelf thickness change dataset (Paolo et. al., 2015). This annual  
223 rate is then applied over the 37 years between 1972 and 2009 to obtain an estimate of the 1972  
224 thickness distribution of the Shackleton Ice Shelf, Denman ice tongue and Scott Glacier. We  
225 refer to this perturbation as ‘ice shelf thinning’ because the majority of the floating portions of  
226 Denman’s ice tongue and Shackleton Ice Shelf have thinned since 1994, although some  
227 sections of Scott Glacier have actually thickened near its calving front (Fig. S3).

228 ii. To represent grounding line retreat since 1972 we advanced Denman’s grounding line  
229 from its position in the 2009 baseline set-up by 10 km to a possible 1972 position (Fig. S3).  
230 We justify a 10 km retreat since 1972 based on the rate of grounding-line retreat observed  
231 between 1996 and 2017 (~5km; Brancato et al., 2020). This can be represented in the model  
232 by either thickening the ice to ground it, or raising the bed into contact with the bottom of the  
233 ice shelf. We have chosen to artificially raise the bedrock to the same height as the bottom of  
234 the ice as the less disruptive method, as changing ice thickness would have an effect on ice  
235 velocity in addition to that caused by moving the grounding line position. For the newly  
236 grounded area, values of the bed slipperiness,  $C$ , are not generated in our model inversion, we  
237 therefore prescribe nearest-neighbour values to those at the grounding line in the model  
238 inversion.

239 iii. To represent the pinning of Denman’s ice tongue against Chugunov Island in the 1972  
240 observations (e.g. Fig. 4d, e), we artificially raise a small area of bedrock on the edge of  
241 Chugunov Island (Fig. S3). Bed slipperiness was set to a value comparable to that immediately  
242 upstream of the grounding line.

243 These three adjustments are applied, both individually and in combination with each other, to  
244 the baseline model setup to produce seven different simulations (E1-7) which perturb,  
245 respectively:

246 E1. Ice shelf thinning.

247 E2. Grounding line retreat

248 E3. Ice shelf thinning and grounding line retreat

249 E4. Unpinning from Chugunov Island

250 E5. Ice shelf thinning and unpinning from Chugunov Island



251 E6. Grounding line retreat and unpinning from Chugunov Island

252 E7. Ice shelf thinning, grounding line retreat and the unpinning from Chugunov Island

253 Below we compare the instantaneous change in ice velocity arising from each perturbation  
254 experiment to observed changes in velocity, and then use these comparisons to understand the  
255 relative importance of each process in contributing to Denman's behaviour over the past 50  
256 years.

257

#### 258 **4.3. Model results**

259 We show observed 2009 ice speed relative to each simulation which represent possible 1972  
260 ice geometries (E1-7, Fig. 5b-h). In all cases, positive (red) values indicate areas where ice was  
261 flowing faster and negative (blue) values show areas where ice was flowing slower in 2009  
262 relative to each 1972 simulation. Perturbing ice shelf thickness to represent ice shelf thinning  
263 since the 1970s results in higher velocities over both the grounded and floating portions of the  
264 Denman system (E1, Fig. 5b). However, the simulated acceleration on Denman's ice tongue  
265 (E1, Fig. 5b) is much larger than the observed acceleration, with the simulation showing a 50%  
266 acceleration in the area just downstream from the grounding line compared to the observed  
267 20% acceleration between 1972 and 2009 (E1, Fig. 5a). Thus, it would appear that ice shelf  
268 thinning alone, is not consistent with the observed velocity changes on the Denman system.  
269 Perturbing the grounding line to account for a possible grounding line retreat since 1972  
270 simulates comparable changes in ice flow speeds to observations near Denman's grounding  
271 line (E2, Fig. 5c), but it is unable to reproduce the observed increases in ice speed across  
272 Denman's ice tongue (E2, Fig. 5c). Thus, grounding line retreat, alone, is also unable to  
273 reproduce the observed pattern of velocity changes. Ice shelf thinning and retreating the  
274 grounding line results in very similar patterns in ice speed change (E3, Fig. 5d) to that of the  
275 grounding line retreat perturbation experiment (E2).

276 In isolation, simulating the unpinning of Denman's ice tongue from Chugunov Island has a  
277 very limited effect on ice flow speeds, with no change in speed near the grounding line and a  
278 very spatially limited change on the ice tongue (E4; Fig. 5e). However, when combining the  
279 unpinning perturbation with either ice shelf thinning (E5; Fig. 5f) or grounding line retreat (E6;  
280 Fig. 5g), it is clear that the unpinning from Chugunov Island causes an acceleration across  
281 Denman's ice tongue. For experiment 5 this results in an even larger overestimate of ice speed



282 change across Denman’s ice tongue in comparison to experiment 1, which only perturbs ice  
283 shelf thickness. However, for experiment 6 the additional inclusion of the unpinning from  
284 Chugunov Island to grounding line retreat results in a simulated pattern of ice flow speed  
285 change very similar to observations. Specifically the unpinning from Chugunov Island has  
286 caused an acceleration across the ice tongue that was not present in experiment 2. Combining  
287 all three perturbations (E7, Fig. 5h) produces changes in ice velocity that are most comparable  
288 to observations. Both the spatial pattern in ice speed change and the simulated ice speed within  
289 box *D* (Fig. 5i) are very similar to observations for both experiments, and the enhanced  
290 westward bending of the directional component of ice velocity in experiment E7 is more  
291 consistent with the observed westward bending of the ice tongue (e.g. Fig. 2b).

292

## 293 **5. Discussion**

### 294 ***5.1 Variation in Denman Glacier’s calving cycle***

295 Our calving cycle reconstruction, combined with historical observations (Cassin and Wilkes,  
296 1858; Mawson, 1914; 1932) hint that Denman’s multi-decadal high-magnitude calving cycle  
297 has remained broadly similar over the past 200 years. It periodically produces a large tabular  
298 iceberg, which then drifts ~60 km northwards before grounding on an offshore ridge, and  
299 typically remains in place for around 20 years before disintegrating/dispersing. However, more  
300 detailed observations and reconstructions of its past three calving events have shown that there  
301 are clear differences in both the size of icebergs produced and in ice tongue structure through  
302 time (Fig. 2). The large variation (50%) in both the size of iceberg produced and the location  
303 the ice front calved from indicates variability in its calving cycle.

304 Extending observational records for ice shelves that calve at irregular intervals, sizes or  
305 locations is especially important because it helps to distinguish between changes in glacier  
306 dynamics caused by longer-term variations in its calving cycle, and changes in glacier  
307 dynamics forced by climate. For example, there have been large variations in ice flow speed at  
308 the Brunt Ice Shelf over the past 50 years (Gudmundsson et al., 2017), but these large variations  
309 can be explained by internal processes following interactions with local pinning points during  
310 the ice shelf’s calving cycle (Gudmundsson et al., 2017). In contrast, the widespread  
311 acceleration of outlet glaciers in the Amundsen Sea sector (Mouginot et al., 2014) is linked to  
312 enhanced intrusions of warm ocean water increasing basal melt rates (e.g. (Thoma et al., 2008;  
313 Jenkins et al., 2018), leading to ice shelf thinning (Paolo et al., 2015) and grounding line retreat



314 (Rignot et al., 2011a). Thus, in the following section we discuss whether the observed speed-  
315 up of Denman since the 1970s (Fig. 3) is more closely linked to variations in its calving cycle  
316 (e.g. Brunt Ice Shelf) or if it has been driven by climate and ocean forcing (e.g. Amundsen  
317 Sea).

318

### 319 *5.2 What has caused Denman Glacier's acceleration since the 1970s?*

320 We observe a spatially widespread acceleration of both Denman's floating and grounded ice.  
321 This is characterised by a  $17 \pm 4\%$  increase in ice flow speed near the grounding line between  
322 1972 and 2017 (Fig. 3c) and a  $36 \pm 5\%$  acceleration in ice-front advance rate from 1972-2017,  
323 or  $30 \pm 5\%$  increase in ice-front advance rate between 1962 and 2017 (Fig. 3b). Our estimates  
324 of the acceleration in ice front advance rate are of a comparable magnitude to the 36%  
325 acceleration of the ice tongue between 1957 and 2017, based on averaged point estimates across  
326 the ice tongue from repeat aerial surveys (Dolgushin, 1966; Rignot et al., 2019). Taken  
327 together, this suggests a limited change in ice tongue speed between 1957 and 1972, before a  
328 rapid acceleration between 1972 and 2017. However, the rate of acceleration throughout this  
329 period has not been constant (Fig. 3b, c). From 1972 to 1990, observations indicate that ice  
330 accelerated approximately three times faster on the ice tongue (Fig. 3b) and twice as fast at the  
331 grounding line (Fig. 3c) in comparison to accelerations in these areas between 1990-2017.  
332 When comparing these observations against our numerical modelling experiments we find that  
333 a combination of grounding line retreat, changes in ice shelf thickness and the unpinning of ice  
334 from Chugunov Island (Fig. 5h) are all required to explain an acceleration of a comparable  
335 magnitude and spatial pattern across the Denman system.

336 Averaged basal melt rates across the Shackleton/Denman system are comparable to the Getz  
337 Ice Shelf (Depoorter et al., 2013; Rignot et al., 2013). Close to Denman's deep grounding line,  
338 melt rates have been estimated at  $45 \text{ m yr}^{-1}$  (Brancato et al., 2020), suggesting the presence of  
339 modified Circumpolar Deep Water in the ice shelf cavity. At nearby Totten Glacier (Fig. 1a),  
340 wind-driven periodic intrusions of warm water flood the continental shelf and cause increased  
341 basal melt rates (Rintoul et al., 2016; Greene et al., 2017) and grounding line retreat (Li et al.,  
342 2015). It is possible that a similar process may be responsible for some of the observed changes  
343 at Denman Glacier. Hydrographic data collected from the Marine Mammals Exploring the  
344 Oceans Pole to Pole consortium (Treasure et al., 2017) show water temperatures of  $-1.31$  to  $-$   
345  $0.26 \text{ }^\circ\text{C}$  at depths between 550 and 850 m on the continental shelf in front of Denman (Brancato



346 et al., 2020). Thus, whilst not confirmed, there is clear potential for warm water to reach  
347 Denman's grounding zone and enhance melt rates.

348 Recent observations of grounding line migration at Denman have shown a 5 km retreat along  
349 its western flank between 1996 and 2017 (Brancato et al., 2020). However, over this time  
350 period there was a limited change in the speed of Denman (2001-2017;  $3 \pm 2\%$  acceleration;  
351 Fig. 3c) and our time series indicates that the acceleration initiated earlier, at some point  
352 between 1972 and 1990 (Fig. 3c). Reconstructions of the bed topography near the grounding  
353 line of Denman Glacier show that the western flank of Denman's grounding line was resting  
354 on a retrograde slope in 1996, a few kilometres behind a topographic ridge (Brancato et al.,  
355 2020). One possibility is that Denman's grounding line retreat initiated much earlier at some  
356 point in the 1970s in response to increased ocean temperatures enhancing melting of the ice  
357 tongue base. This initial grounding line retreat and possible ocean-induced ice tongue thinning  
358 may have caused the initial rapid acceleration between 1972 and 1990, before continuing at a  
359 slower rate. However, our numerical modelling shows that whilst the combination of the retreat  
360 of Denman's grounding line and ice tongue thinning can produce a similar magnitude of  
361 acceleration near the grounding line to observations (E3; Fig. 5e), these modelled processes  
362 cannot explain the widespread acceleration across the ice tongue (e.g. E4; Fig. 5d).

363 In order to simulate a comparable spatial acceleration across both Denman's grounded and  
364 floating ice to observations, the un-pinning of ice from Chugunov Island following Denman's  
365 last calving event in 1984 is required (e.g. E6 & 7; Fig. 5g, 5h). In isolation, the reduction in  
366 contact with Chugunov Island has had no effect on ice flow speeds at both Denman's grounding  
367 line and ice tongue (E4; Fig. 5d). However, when combined with grounding line retreat and ice  
368 tongue thinning, the spatial pattern of simulated ice speed change across the ice tongue more  
369 closely resemble observations (E6 & 7; Fig. 5g, 5h). Specifically, the unpinning of the ice  
370 tongue from Chugunov Island has caused an acceleration across much of Denman's ice tongue.  
371 The most likely explanation as to why the unpinning from Chugunov Island only influences  
372 ice speed patterns in combination with ice tongue thinning and grounding line retreat, and not  
373 in isolation, is that ice tongue thinning and grounding line retreat have caused a change in the  
374 direction of flow of the ice tongue since the 1970s. In all simulations that perturb either ice  
375 tongue thickness or retreat the grounding line (Fig. 5b, c, e, f, g, h), there is a clear westward  
376 bending in ice flow direction near Chugunov Island which results in a reduction in contact  
377 between the ice tongue and Chugunov Island. This is consistent with observations that show a  
378 distinctive westward bending of Denman's ice tongue since the 1970s (Fig. 2b). These findings



379 therefore suggest that the reduction in contact with Chugunov Island following Denman's  
380 calving event in 1984 caused an instantaneous acceleration across large sections of its ice  
381 tongue, meaning that this calving event has had a direct impact on the spatial pattern of  
382 acceleration observed between 1972 and 2017. However, because of the westward bending of  
383 Denman's ice tongue during its re-advance following its 1984 calving event, the ice tongue  
384 now makes limited contact with Chugunov Island (e.g. Fig. 4e) and has a very limited effect  
385 on ice flow speeds (e.g. E4; Fig. 5e).

386 The acceleration of Denman's ice tongue following its last major calving event in 1984 may  
387 have also caused a series of positive feedbacks resulting in further acceleration. We observe a  
388 steepening of the velocity gradient across Denman's shear margins and a pattern of the  
389 acceleration of the dominant Denman ice tongue and slowdown of the neighbouring Shackleton  
390 Ice Shelf and Scott Glacier (Fig. 3a). We also observe the lateral migration of the shear margins  
391 at sub-decadal timescales (Fig. 3e). These distinctive patterns in ice speed change are very  
392 similar to those reported at the Stamcomb-Wills Ice Shelf (Humbert et al., 2009) and between  
393 the Thwaites Ice Tongue and Eastern Ice Shelf (Mouginot et al., 2014; Miles et al., 2020), and  
394 are symptomatic of a weakening of shear margins. Therefore, we suggest that at Denman, after  
395 the initial acceleration following the reduction in contact with Chugunov Island, the shear  
396 margins may have weakened causing further acceleration. We do not include this process in  
397 our numerical experiments, and it may explain the divergence between observations and  
398 simulated ice speed change in the neighbouring Shackleton Ice Shelf and Scott Glacier (Fig.  
399 3a; Fig. 5).

400 Overall, our observations and numerical simulations suggest that the cause of Denman's  
401 acceleration since the 1970s is complex and likely reflects a combination of processes linked  
402 to the ocean and a reconfiguration of Denman's ice tongue. One possibility is that the  
403 acceleration of ice across Denman's grounding line has almost entirely been driven by warm  
404 ocean forcing driving grounding line retreat and ice tongue thinning, with the unpinning of  
405 Denman's ice tongue from Chugunov Island only causing a localised acceleration across  
406 floating ice. An alternative explanation is that warm ocean forcing has caused ice tongue  
407 thinning and grounding line retreat, but the acceleration behind the grounding line has been  
408 enhanced through time by changes in ice tongue configuration. Either way, our results highlight  
409 that both oceanic processes and the changes in ice tongue structure associated with Denman's  
410 calving event have been important in causing Denman's observed acceleration.



411

### 412 **5.3 Future evolution of Denman Glacier**

413 In the short-term, an important factor in the evolution of the wider Denman/Shackleton system  
414 is Denman's next calving event. Whilst our observations do not suggest that a calving event is  
415 imminent (next 1-2 years), our calving cycle reconstruction indicates that a calving event at  
416 some point in the 2020s is highly likely. Because the calving cycle of Denman Glacier has  
417 demonstrated some variability in the past (e.g. Fig. 2), the precise geometry of its ice tongue  
418 after this calving event cannot be accurately predicted. In particular, it is unclear how  
419 Denman's ice tongue will realign in relation to Chugunov Island following its next calving  
420 event. For example, if following Denman's next calving event the direction of ice flow shifts  
421 eastwards to a similar configuration to the 1970s and the ice tongue makes contact with  
422 Chugunov Island, the increased resistance could slowdown Denman's ice tongue for the  
423 duration of its calving cycle, but it is unclear if any slowdown could propagate to the grounding  
424 line. Thus, this event may have important implications for the evolution of the  
425 Denman/Shackleton system for multiple decades.

426 In the medium-term (next 50 years) atmospheric warming could also have a direct impact on  
427 the stability of the Denman/Shackleton system. Following the collapse of Larsen B in 2002,  
428 Shackleton is now the most northerly major ice shelf remaining in Antarctica, with most of the  
429 ice shelf lying outside the Antarctic Circle. Numerous surface meltwater features have been  
430 repeatedly reported on its surface (Kingslake et al., 2017; Stokes et al., 2019; Arthur et al.,  
431 2020). There is no evidence that these features currently have a detrimental impact on its  
432 stability, but there is a possibility that projected increases in surface melt (Trusel et al., 2015)  
433 could increase the ice shelves vulnerability to meltwater-induced hydrofracturing

434

### 435 **6. Conclusion**

436 We have reconstructed Denman Glacier's calving cycle to show that its previous two calving  
437 events (~1940s and 1984) have varied in size by 50% and there have been clear differences in  
438 ice tongue structure, with a notable unpinning from Chugunov Island following the 1984  
439 calving event. We also observe a long-term acceleration of Denman Glacier across both  
440 grounded and floating sections of ice, with both the ice front advance rate and ice near the  
441 grounding line accelerating by  $36 \pm 5\%$  and  $17 \pm 4\%$ , respectively, between 1972 and 2017. We



442 show that in order to simulate a post-1972 acceleration that is comparable with observations,  
443 its grounding line must have retreated since the 1970s. We also highlight the importance of the  
444 reconfiguration of the Denman ice tongue system in determining the spatial pattern of  
445 acceleration observed.

446 The recent changes in the Denman system are important because Denman's grounding line  
447 currently rests on a retrograde slope which extends 50 km into its basin (Morlighem et al.,  
448 2019; Brancato et al., 2020), suggesting clear potential for marine ice sheet instability. Given  
449 the large catchment size, it has potential to make globally significant contributions to mean sea  
450 level rise in the coming decades (1.49 m; Morlighem et al., 2020). Crucial to assessing the  
451 magnitude of any future sea level contributions is improving our understanding of regional  
452 oceanography, and determining whether the observed changes at Denman are the consequence  
453 of a longer-term ocean warming. This is in addition to monitoring and understanding the  
454 potential impact of any future changes in the complex Shackleton/Denman ice shelf system.

455 In a wider context our results add to the growing body of evidence that some major East  
456 Antarctic outlet glaciers, with multi-meter sea-level equivalent catchments have responded to  
457 changes in ocean-climate forcing over the past 100 years and, therefore, will be sensitive to  
458 projected future warming. The Ninnis Ice Tongue has retreated (Frezzotti et al., 1998), part of  
459 the Cook Ice Shelf has collapsed (Miles et al., 2018) and Totten's grounding line is retreating  
460 (Li et al., 2015), and it has been losing mass for several decades (Rignot et al., 2019). However,  
461 despite recent improvements (e.g. Morlighem et al., 2020), our understanding of bed  
462 topography, oceanography, bathymetry and ice shelf cavity geometry in these key regions of  
463 East Antarctic still lag behind that of other regions e.g. Amundsen Sea sector, making the  
464 accurate assessment of the magnitude and rates of future sea level contributions challenging.

465

#### 466 **Acknowledgements**

467 This work was funded by the Natural Environment Research Council (grant number:  
468 NE/R000824/1). Landsat and the declassified historical imagery from 1962 is freely available  
469 and can be downloaded via Earth Explorer (<https://earthexplorer.usgs.gov/>). COSI-Corr is  
470 available at [http://www.tectonics.caltech.edu/slip\\_history/spot\\_coseis/download\\_software](http://www.tectonics.caltech.edu/slip_history/spot_coseis/download_software.html)  
471 .html. The source code for Úa is available at <https://doi.org/10.5281/zenodo.3706624>.  
472 MEaSURES annual ice velocity maps are available at  
473 <https://doi.org/10.5067/9T4EPQXTJYW9>. We also thank Eric Rignot for providing digitized



474 estimates of ice flow speed across parts of Denman's ice tongue, based on the mapped estimates  
475 of Dolgushin et al. (1966).

476

#### 477 **References**

478 Aitken, A. R. A., Roberts, J. L., van Ommen, T. D., Young, D. A., Golledge, N. R., Greenbaum,  
479 J. S., Blankenship, D. D., and Siegert, M. J.: Repeated large-scale retreat and advance of  
480 Totten Glacier indicated by inland bed erosion, *Nature*, 533, 385–+, 2016.

481 Arthur, J. F., Stokes, C. R., Jamieson, S. S. R., Carr, J. R., and Leeson, A. A.: Distribution and  
482 seasonal evolution of supraglacial lakes on Shackleton Ice Shelf, East Antarctica, *The*  
483 *Cryosphere Discuss.*, <https://doi.org/10.5194/tc-2020-101>, in review, 2020.

484 Brancato, V., Rignot, E., Milillo, P., Morlighem, M., Mouginot, J., An, L., Scheuchl, B., Jeong,  
485 S., Rizzoli, P., Bueso Bello, J. L., and Prats-Iraola, P.: Grounding line retreat of Denman  
486 Glacier, East Antarctica, measured with COSMO-SkyMed radar interferometry data,  
487 *Geophys Res Lett*, n/a, e2019GL086291.

488 Burke, K. D., Williams, J. W., Chandler, M. A., Haywood, A. M., Lunt, D. J., and Otto-  
489 Bliesner, B. L.: Pliocene and Eocene provide best analogs for near-future climates, *P Natl*  
490 *Acad Sci USA*, 115, 13288–13293, 2018.

491 Cassin, John, and Charles Wilkes. *United States Exploring Expedition: During the Years 1838,*  
492 *1839, 1840, 1841, 1842, Under the Command of Charles Wilkes, USN. Mammalogy and*  
493 *Ornithology.* JB Lippincott & Company, 1858.

494 Cuffey, K.M. and W.S.B. Paterson. *The physics of glaciers.* Fourth edition. Amsterdam, etc.,  
495 Academic Press. 704pp. ISBN-10: 0-123694-61-2, ISBN-13: 978-0-123-69461-4,  
496 hardback, £60.99/€71.95/US\$99.95. *Journal of Glaciology*, 57(202), 383–384.  
497 doi:10.3189/002214311796405906, 2010.

498 DeConto, R. M. and Pollard, D.: Contribution of Antarctica to past and future sea-level rise,  
499 *Nature*, 531, 591–+, 2016.

500 Depoorter, M. A., Bamber, J. L., Griggs, J. A., Lenaerts, J. T. M., Ligtenberg, S. R. M., van  
501 den Broeke, M. R., and Moholdt, G.: Calving fluxes and basal melt rates of Antarctic ice  
502 shelves, *Nature*, 502, 89–+, 2013.

503 Dolgushin, L. D. "New data on the rates of movement of Antarctic glaciers." *Soviet Antarctic*  
504 *Expedition Information Bulletin* 55 (1966): 41–42.

505 Flament, T. and Remy, F.: Dynamic thinning of Antarctic glaciers from along-track repeat  
506 radar altimetry, *J Glaciol*, 58, 830–840, 2012.

507 Frezzotti, M., Cimbelli, A., and Ferrigno, J. G.: Ice-front change and iceberg behaviour along  
508 Oates and George V Coasts, Antarctica, 1912–96, *Annals of Glaciology*, Vol 27, 1998, 27,  
509 643–650, 1998.



- 510 Gardner, A. S., Moholdt, G., Scambos, T., Fahnestock, M., Ligtenberg, S., van den Broeke, M.,  
511 and Nilsson, J.: Increased West Antarctic and unchanged East Antarctic ice discharge over  
512 the last 7 years, *Cryosphere*, 12, 521-547, 2018.
- 513 Gasson, E., DeConto, R., and Pollard, D.: Antarctic bedrock topography uncertainty and ice  
514 sheet stability, *Geophys Res Lett*, 42, 5372-5377, 2015.
- 515 Golleddge, N. R., Kowalewski, D. E., Naish, T. R., Levy, R. H., Fogwill, C. J., and Gasson, E.  
516 G. W.: The multi-millennial Antarctic commitment to future sea-level rise, *Nature*, 526,  
517 421-+, 2015.
- 518 Greenbaum, J. S., Blankenship, D. D., Young, D. A., Richter, T. G., Roberts, J. L., Aitken, A.  
519 R. A., Legresy, B., Schroeder, D. M., Warner, R. C., van Ommen, T. D., and Siegert, M. J.:  
520 Ocean access to a cavity beneath Totten Glacier in East Antarctica, *Nat Geosci*, 8, 294-298,  
521 2015.
- 522 Greene, C. A., Blankenship, D. D., Gwyther, D. E., Silvano, A., and van Wijk, E.: Wind causes  
523 Totten Ice Shelf melt and acceleration, *Science Advances*, 3, 2017.
- 524 Gudmundsson, G. H.: Ice-shelf buttressing and the stability of marine ice sheets, *Cryosphere*,  
525 7, 647-655, 2013.
- 526 Gudmundsson, G. H., de Rydt, J., and Nagler, T.: Five decades of strong temporal variability  
527 in the flow of Brunt Ice Shelf, Antarctica, *J Glaciol*, 63, 164-175, 2017.
- 528 Gudmundsson, G. H., Krug, J., Durand, G., Favier, L., and Gagliardini, O.: The stability of  
529 grounding lines on retrograde slopes, *Cryosphere*, 6, 1497-1505, 2012.
- 530 Gudmundsson, G. H., Paolo, F. S., Adusumilli, S., & Fricker, H. A. Instantaneous Antarctic  
531 ice- sheet mass loss driven by thinning ice shelves. *Geophysical Research Letters*, 46,  
532 13903– 13909. <https://doi.org/10.1029/2019GL085027>, 2019
- 533 Helm, V., Humbert, A., and Miller, H.: Elevation and elevation change of Greenland and  
534 Antarctica derived from CryoSat-2, *Cryosphere*, 8, 1539-1559, 2014.
- 535 Hill, E. A., Gudmundsson, G. H., Carr, J. R., and Stokes, C. R.: Velocity response of Petermann  
536 Glacier, northwest Greenland, to past and future calving events, *The Cryosphere*, 12, 3907–  
537 3921, <https://doi.org/10.5194/tc-12-3907-2018>, 2018.
- 538 Humbert, A., Kleiner, T., Mohrholz, C. O., Oelke, C., Greve, R., and Lange, M. A.: A  
539 comparative modeling study of the Brunt Ice Shelf/Stancomb-Wills Ice Tongue system, East  
540 Antarctica, *J Glaciol*, 55, 53-65, 2009.
- 541 Jenkins, A., Shoosmith, D., Dutrieux, P., Jacobs, S., Kim, T. W., Lee, S. H., Ha, H. K., and  
542 Stammerjohn, S.: West Antarctic Ice Sheet retreat in the Amundsen Sea driven by decadal  
543 oceanic variability, *Nat Geosci*, 11, 733-+, 2018.



- 544 King, M. A., Bingham, R. J., Moore, P., Whitehouse, P. L., Bentley, M. J., and Milne, G. A.:  
545 Lower satellite-gravimetry estimates of Antarctic sea-level contribution, *Nature*, 491, 586-  
546 +, 2012.
- 547 Kingslake, J., Ely, J. C., Das, I., and Bell, R. E.: Widespread movement of meltwater onto and  
548 across Antarctic ice shelves, *Nature*, 544, 349-+, 2017.
- 549 Lea, J. M.: The Google Earth Engine Digitisation Tool (GEEDiT) and the Margin change  
550 Quantification Tool (MaQiT) - simple tools for the rapid mapping and quantification of  
551 changing Earth surface margins, *Earth Surf Dynam*, 6, 551-561, 2018.
- 552 Leprince, S., Ayoub, F., Klinger, Y., and Avouac, J. P.: Co-Registration of Optically Sensed  
553 Images and Correlation (COSI-Corr): an operational methodology for ground deformation  
554 measurements, *Igarss: 2007 Ieee International Geoscience and Remote Sensing*  
555 *Symposium*, Vols 1-12, doi: 10.1109/Igarss.2007.4423207, 2007. 1943-+, 2007.
- 556 Levermann, A., Winkelmann, R., Albrecht, T., Goelzer, H., Golledge, N. R., Greve, R.,  
557 Huybrechts, P., Jordan, J., Leguy, G., Martin, D., Morlighem, M., Pattyn, F., Pollard, D.,  
558 Quiquet, A., Rodehacke, C., Seroussi, H., Sutter, J., Zhang, T., Van Breedam, J., Calov, R.,  
559 DeConto, R., Dumas, C., Garbe, J., Gudmundsson, G. H., Hoffman, M. J., Humbert, A.,  
560 Kleiner, T., Lipscomb, W. H., Meinshausen, M., Ng, E., Nowicki, S. M. J., Perego, M.,  
561 Price, S. F., Saito, F., Schlegel, N.-J., Sun, S., and van de Wal, R. S. W.: Projecting  
562 Antarctica's contribution to future sea level rise from basal ice shelf melt using linear  
563 response functions of 16 ice sheet models (LARMIP-2), *Earth Syst. Dynam.*, 11, 35–76,  
564 <https://doi.org/10.5194/esd-11-35-2020>, 2020.
- 565 Li, X., Rignot, E., Morlighem, M., Mouginot, J., and Scheuchl, B.: Grounding line retreat of  
566 Totten Glacier, East Antarctica, 1996 to 2013, *Geophys Res Lett*, 42, 8049-8056, 2015.
- 567 Li, X., Rignot, E., and Mouginot, J.: Ice flow dynamics and mass loss of Totten Glacier, East  
568 Antarctica, from 1989 to 2015, *Geophys Res Lett*, 43, 6366-6373, 2016.
- 569 Mawson, D., *The Home of the Blizzard*, Heinemann, London, 1915.
- 570 Mawson, Douglas. "The BANZ Antarctic Research Expedition, 1929-31." *The Geographical*  
571 *Journal* 80.2 (1932): 101-126.
- 572 Miles, B. W. J., Stokes, C. R., and Jamieson, S. S. R.: Pan-ice-sheet glacier terminus change  
573 in East Antarctica reveals sensitivity of Wilkes Land to sea-ice changes, *Science Advances*,  
574 2, 2016.
- 575 Miles, B. W. J., Stokes, C. R., and Jamieson, S. S. R.: Velocity increases at Cook Glacier, East  
576 Antarctica, linked to ice shelf loss and a subglacial flood event, *Cryosphere*, 12, 3123-3136,  
577 2018.



- 578 Miles, B. W. J., Stokes, C. R., Jenkins, A., Jordan, J. R., Jamieson, S. S. R., and Gudmundsson,  
579 G. H.: Intermittent structural weakening and acceleration of the Thwaites Glacier Tongue  
580 between 2000 and 2018, *J Glaciol*, 66, 485-495, 2020.
- 581 Miles, B. W. J., Stokes, C. R., Vieli, A., and Cox, N. J.: Rapid, climate-driven changes in outlet  
582 glaciers on the Pacific coast of East Antarctica, *Nature*, 500, 563-+, 2013.
- 583 Mohajerani, Y., Velicogna, I., and Rignot, E.: Evaluation of Regional Climate Models Using  
584 Regionally Optimized GRACE Mascons in the Amery and Getz Ice Shelves Basins,  
585 Antarctica, *Geophys Res Lett*, 46, 13883-13891, 2019.
- 586 Moon, T. and Joughin, I.: Changes in ice front position on Greenland's outlet glaciers from  
587 1992 to 2007, *J Geophys Res-Earth*, 113, 2008.
- 588 Morlighem, M., Rignot, E., Binder, T., Blankenship, D., Drews, R., Eagles, G., Eisen, O.,  
589 Ferraccioli, F., Forsberg, R., Fretwell, P., Goel, V., Greenbaum, J. S., Gudmundsson, H.,  
590 Guo, J. X., Helm, V., Hofstede, C., Howat, I., Humbert, A., Jokat, W., Karlsson, N. B., Lee,  
591 W. S., Matsuoka, K., Millan, R., Mouginot, J., Paden, J., Pattyn, F., Roberts, J., Rosier, S.,  
592 Ruppel, A., Seroussi, H., Smith, E. C., Steinhage, D., Sun, B., van den Broeke, M. R., van  
593 Ommen, T. D., van Wessem, M., and Young, D. A.: Deep glacial troughs and stabilizing  
594 ridges unveiled beneath the margins of the Antarctic ice sheet, *Nat Geosci*, 13, 132-+, 2020.
- 595 Mouginot, J., Rignot, E., and Scheuchl, B.: Sustained increase in ice discharge from the  
596 Amundsen Sea Embayment, West Antarctica, from 1973 to 2013, *Geophys Res Lett*, 41,  
597 1576-1584, 2014.
- 598 Mouginot, J., Rignot, E., Scheuchl, B., and Millan, R.: Comprehensive Annual Ice Sheet  
599 Velocity Mapping Using Landsat-8, Sentinel-1, and RADARSAT-2 Data, *Remote Sens-*  
600 *Basel*, 9, 2017.
- 601 Paolo, F. S., Fricker, H. A., and Padman, L.: Volume loss from Antarctic ice shelves is  
602 accelerating, *Science*, doi: 10.1126/science.aaa0940, 2015. 2015.
- 603 Pritchard, H. D., Arthern, R. J., Vaughan, D. G., and Edwards, L. A.: Extensive dynamic  
604 thinning on the margins of the Greenland and Antarctic ice sheets, *Nature*, 461, 971-975,  
605 2009.
- 606 Pattyn, F., Perichon, L., Aschwanden, A., Breuer, B., de Smedt, B., Gagliardini, O.,  
607 Gudmundsson, G. H., Hindmarsh, R. C. A., Hubbard, A., Johnson, J. V., Kleiner, T.,  
608 Konovalov, Y., Martin, C., Payne, A. J., Pollard, D., Price, S., Rückamp, M., Saito, F.,  
609 Souček, O., Sugiyama, S., and Zwinger, T.: Benchmark experiments for higher-order and  
610 full-Stokes ice sheet models (ISMIP-HOM), *The Cryosphere*, 2, 95-108,  
611 <https://doi.org/10.5194/tc-2-95-2008>, 2008.
- 612 Pattyn, F., Schoof, C., Perichon, L., Hindmarsh, R. C. A., Bueler, E., de Fleurian, B., Durand,  
613 G., Gagliardini, O., Gladstone, R., Goldberg, D., Gudmundsson, G. H., Huybrechts, P., Lee,



- 614 V., Nick, F. M., Payne, A. J., Pollard, D., Rybak, O., Saito, F., and Vieli, A.: Results of the  
615 Marine Ice Sheet Model Intercomparison Project, MISIMIP, *The Cryosphere*, 6, 573–588,  
616 <https://doi.org/10.5194/tc-6-573-2012>, 2012.
- 617 Rignot, E., Jacobs, S., Mouginot, J., and Scheuchl, B.: Ice-Shelf Melting Around Antarctica,  
618 *Science*, 341, 266-270, 2013.
- 619 Rignot, E., Mouginot, J., and Scheuchl, B.: Antarctic grounding line mapping from differential  
620 satellite radar interferometry, *Geophys Res Lett*, 38, 2011a.
- 621 Rignot, E., Mouginot, J., and Scheuchl, B.: Ice Flow of the Antarctic Ice Sheet, *Science*, 333,  
622 1427-1430, 2011b.
- 623 Rignot, E., Mouginot, J., Scheuchl, B., van den Broeke, M., van Wessem, M. J., and  
624 Morlighem, M.: Four decades of Antarctic Ice Sheet mass balance from 1979-2017, *P Natl*  
625 *Acad Sci USA*, 116, 1095-1103, 2019.
- 626 Rintoul, S. R., Silvano, A., Pena-Molino, B., van Wijk, E., Rosenberg, M., Greenbaum, J. S.,  
627 and Blankenship, D. D.: Ocean heat drives rapid basal melt of the Totten Ice Shelf, *Science*  
628 *Advances*, 2, 2016.
- 629 Ritz, C., Edwards, T. L., Durand, G., Payne, A. J., Peyaud, V., and Hindmarsh, R. C. A.:  
630 Potential sea-level rise from Antarctic ice-sheet instability constrained by observations,  
631 *Nature*, 528, 115-+, 2015.
- 632 Scherer, R. P., DeConto, R. M., Pollard, D., and Alley, R. B.: Windblown Pliocene diatoms  
633 and East Antarctic Ice Sheet retreat, *Nat Commun*, 7, 2016.
- 634 Scherler, D., Leprince, S., and Strecker, M. R.: Glacier-surface velocities in alpine terrain from  
635 optical satellite imagery - Accuracy improvement and quality assessment, *Remote Sens*  
636 *Environ*, 112, 3806-3819, 2008.
- 637 Schoof, C.: Ice sheet grounding line dynamics: Steady states, stability, and hysteresis, *J*  
638 *Geophys Res-Earth*, 112, 2007.
- 639 Schröder, L., Horwath, M., Dietrich, R., and Helm, V.: Four decades of surface elevation  
640 change of the Antarctic Ice Sheet from multi-mission satellite altimetry, *The Cryosphere*  
641 *Discuss.*, 2018, 1-25, 2018.
- 642 Shen, Q., Wang, H. S., Shum, C. K., Jiang, L. M., Hsu, H. T., and Dong, J. L.: Recent high-  
643 resolution Antarctic ice velocity maps reveal increased mass loss in Wilkes Land, East  
644 Antarctica, *Sci Rep-Uk*, 8, 2018.
- 645 Stokes, C. R., Sanderson, J. E., Miles, B. W. J., Jamieson, S. S. R., and Leeson, A. A.:  
646 Widespread distribution of supraglacial lakes around the margin of the East Antarctic Ice  
647 Sheet. *Sci Rep* 9, 13823, 2019.
- 648 Thoma, M., Jenkins, A., Holland, D., and Jacobs, S.: Modelling Circumpolar Deep Water  
649 intrusions on the Amundsen Sea continental shelf, Antarctica, *Geophys Res Lett*, 35, 2008.



650 Trusel, L. D., Frey, K. E., Das, S. B., Karnauskas, K. B., Munneke, P. K., van Meijgaard, E.,  
651 and van den Broeke, M. R.: Divergent trajectories of Antarctic surface melt under two  
652 twenty-first-century climate scenarios, *Nat Geosci*, 8, 927-U956, 2015.

653 Vogel, C. R. *Computational methods for inverse problems*. Vol. 23. Siam, 2002.

654 Williams, T., van de Flierdt, T., Hemming, S. R., Chung, E., Roy, M., and Goldstein, S. L.:  
655 Evidence for iceberg armadas from East Antarctica in the Southern Ocean during the late  
656 Miocene and early Pliocene, *Earth Planet Sc Lett*, 290, 351-361, 2010.

657 Young, D. A., Lindzey, L. E., Blankenship, D. D., Greenbaum, J. S., de Gorord, A. G., Kempf,  
658 S. D., Roberts, J. L., Warner, R. C., Van Ommen, T., Siegert, M. J., and Le Meur, E.: Land-  
659 ice elevation changes from photon-counting swath altimetry: first applications over the  
660 Antarctic ice sheet, *J Glaciol*, 61, 17-28, 2015.

661 Young, D. A., Wright, A. P., Roberts, J. L., Warner, R. C., Young, N. W., Greenbaum, J. S.,  
662 Schroeder, D. M., Holt, J. W., Sugden, D. E., Blankenship, D. D., van Ommen, T. D., and  
663 Siegert, M. J.: A dynamic early East Antarctic Ice Sheet suggested by ice-covered fjord  
664 landscapes, *Nature*, 474, 72-75, 2011.

665 Weertman J., Stability of the junction of an ice sheet and an ice shelf. *J. Glaciol.*, 13(67), 3–11,  
666 1974.

667

668

669

670

671

672

673

674

675

676

677

678

679

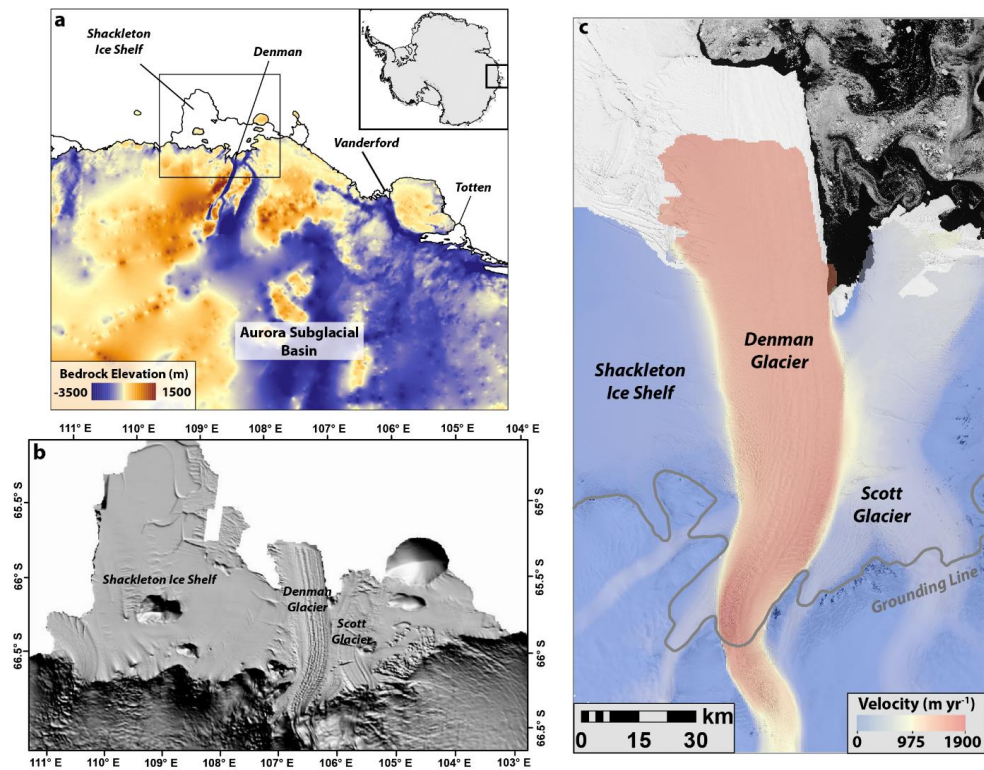
680

681

682

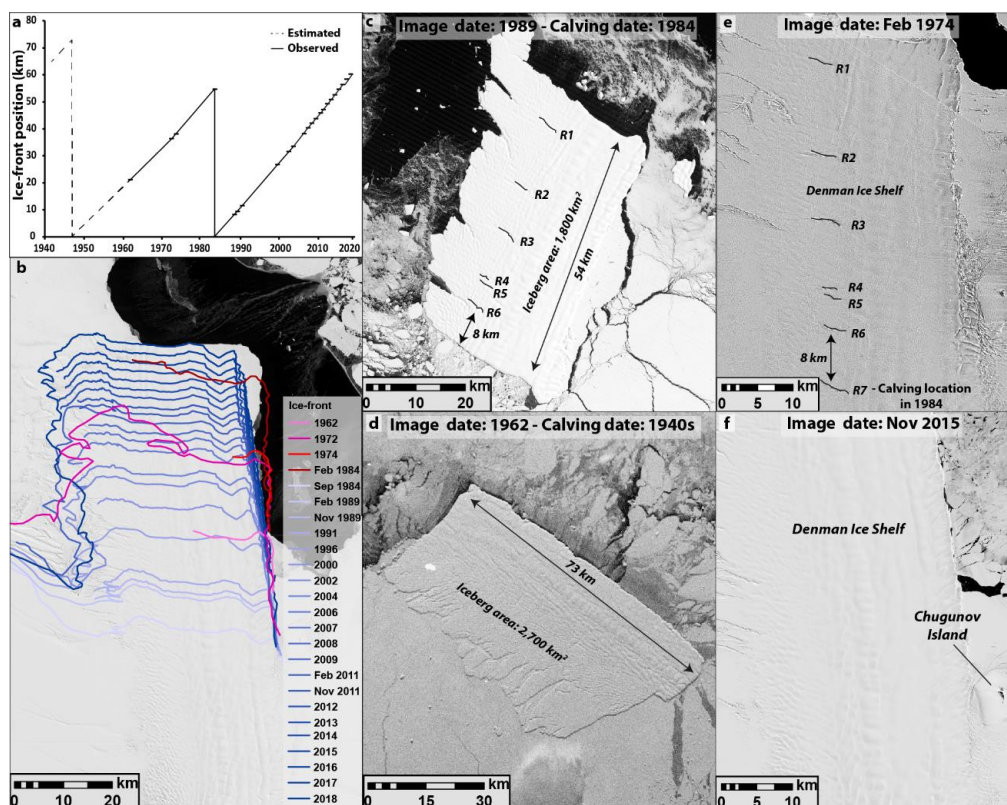


683 **Figures**



6

685 **Figure 1:** a) Bedrock elevation of the Aurora Subglacial Basin (Morlighem et al., 2020). Note  
686 the deep trough inland of the Denman grounding line. b) REMA hill-shade DEM of Denman  
687 Glacier, Scott Glacier, and the Shackleton Ice Shelf (Howat et al., 2019). Note the complex  
688 composition of the Shackleton Ice Shelf with several pinning points. c) MEaSUREs velocity  
689 of Denman Glacier (Rignot et al., 2011) overlain on a Landsat-8 image from November 2018.  
690 Note the steep velocity gradient between the Shackleton Ice Shelf, Denman Glacier and  
691 Scott Glacier.



692

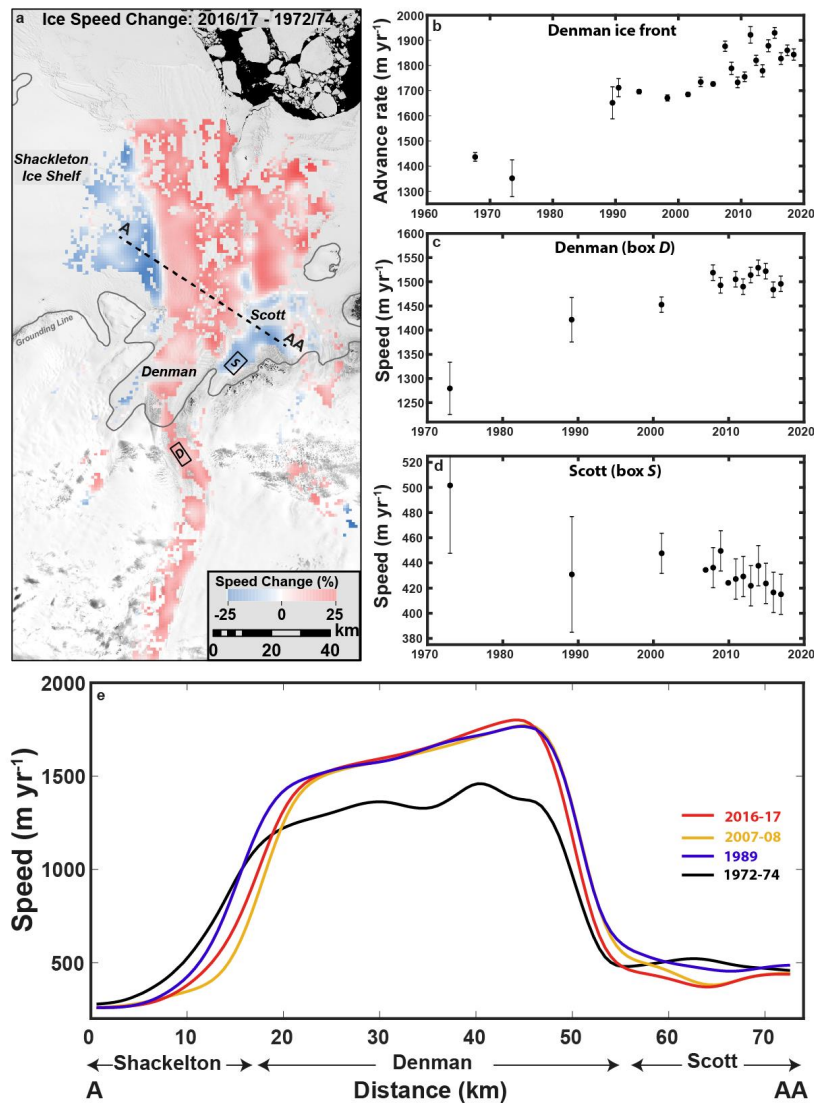
693

694

695 **Figure 2:** a) Reconstructed calving cycle of Denman Glacier 1940-2018. b) Examples of ice-  
696 front mapping 1962-2018. Note the change in angle of the ice shelf between its present (light  
697 blue – dark blue lines) and previous (pink-red lines) calving cycle. c) and d) Images of the  
698 grounded iceberg produced by Denman in 1984 (c) and in the 1940s (d). e) and f) Difference  
699 in ice shelf morphology between 1974 and 2015. Note the presence of rifting in e (digitized in  
700 black).

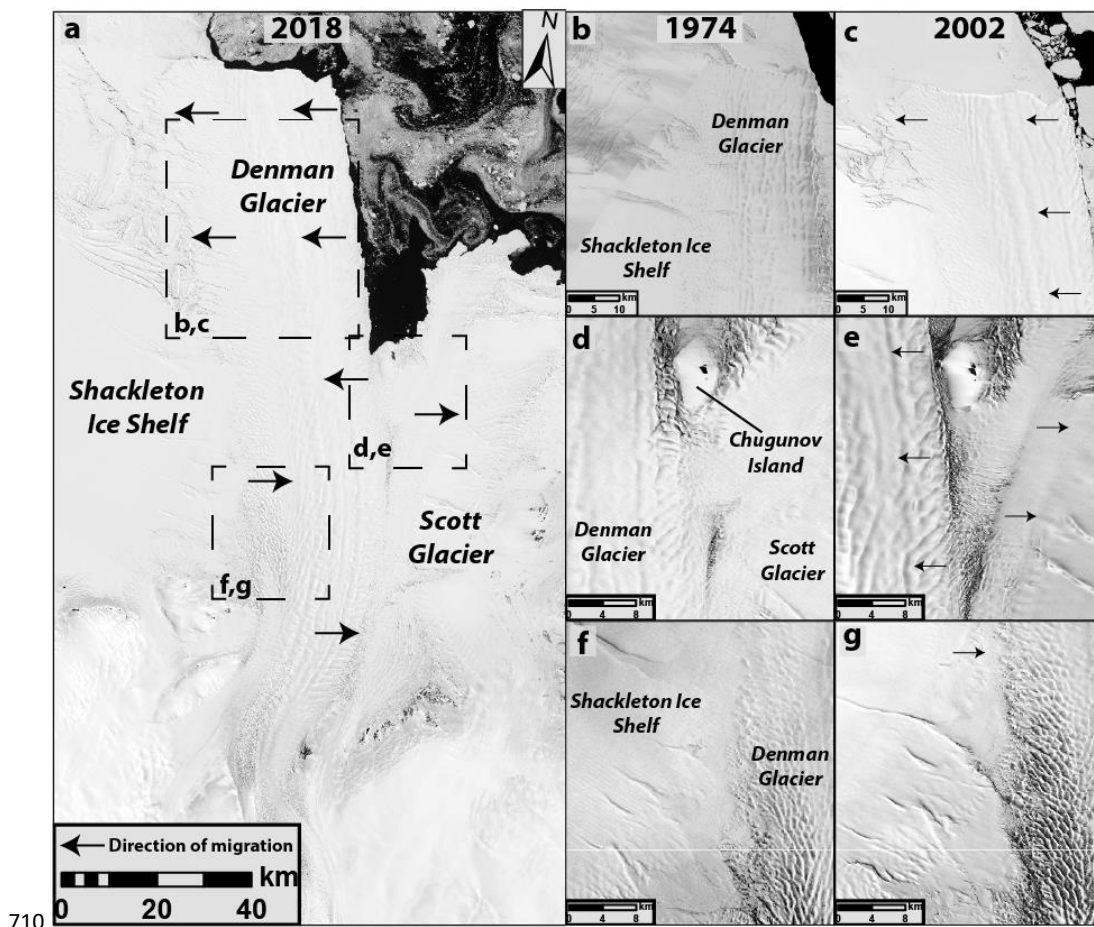
701

702



703

704 **Figure 3:** a) Percentage difference in ice speed between 2016-17 and 1972-74. Red indicates  
 705 a relative increase in 2016-17 and blue a relative decrease in 2016-17. b) Time series of the  
 706 advance rate of the Denman ice-front 1962-2018. c) Time series of mean ice speed from box  
 707 D, (1972-2017) approximately 10 km behind the Denman grounding line. d) Time series of  
 708 mean ice speed from box S, on Scott Glacier, 1972-2017. e) Ice speed profiles across the  
 709 Shackleton-Denman-Scott system from 1972-74, 1989, 2007-08 and 2016-17.



710

711 **Figure 4:** a) Direction of ice tongue migration since 1974. b), d) and f) Close-up in examples  
712 of ice tongue structure and location in 1974. c), e) and g) Close-up in examples of ice tongue  
713 structure and position in 2002. In particular, note the reduction in contact between Denman  
714 Glacier and Chugunov Island between 1974 (d) and 2002 (e).

715

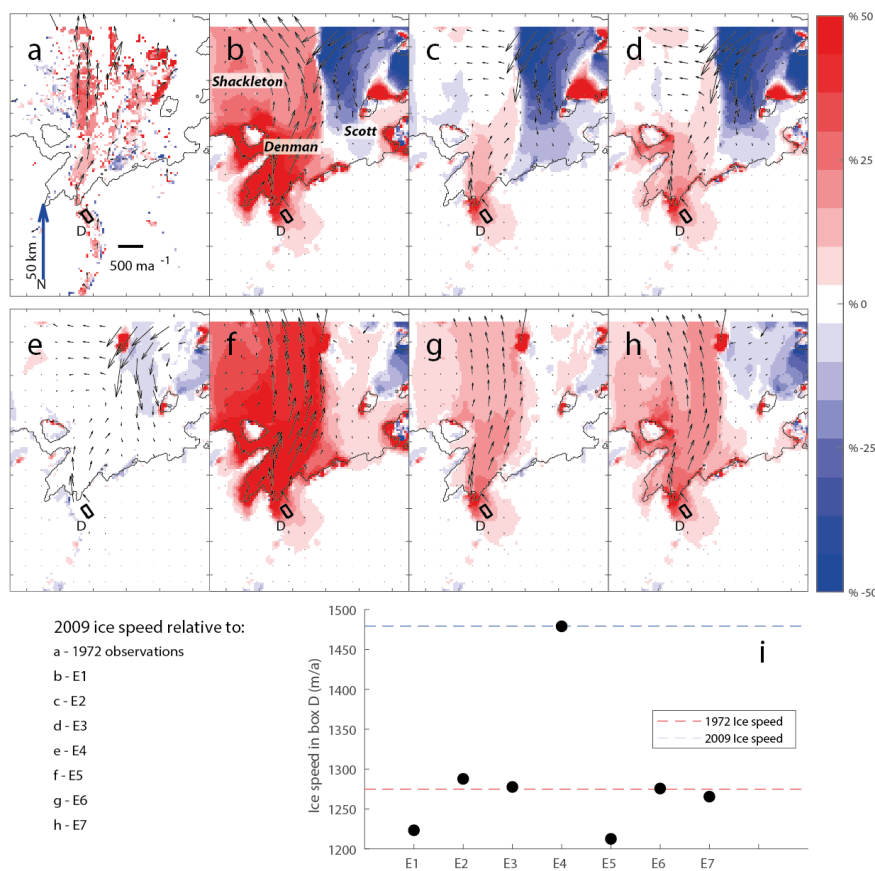
716

717

718

719

720



721

722 **Figure 5 – The effect of varying ice geometry on ice flow:** Ice velocity difference between  
 723 2009 observations and **a)** observations from 1972, and **b)-h)** seven experiments which perturb  
 724 2009 ice geometry to represent possible 1972 ice geometry configurations. The seven  
 725 experiments are: **b)** ice shelf thinning (E1), **c)** grounding line retreat (E2), **d)** ice shelf thinning  
 726 and grounding line retreat (E3), **e)** unpinning from Chugunov Island (E4), **f)** ice shelf thinning  
 727 and unpinning from Chugunov Island (E5), **g)** grounding line retreat and unpinning from  
 728 Chugunov Island (E6) and **h)** combining ice shelf thinning, grounding line retreat and the  
 729 unpinning from Chugunov Island (E7). Note that red indicates areas where ice is flowing faster  
 730 in 2009 and blue indicates areas that are flowing slower with arrows showing the direction and  
 731 magnitude of change when compared to the 1972 perturbations. Finally, **i)** the mean speed in  
 732 box D (located just upstream of the grounding line, shown in black) in the perturbed (1972)  
 733 configuration, with the observed 1972 and 2009 speed shown in red and blue, respectively. E7  
 734 most closely matches the speed observed in box D, the spatial pattern of the observed  
 735 acceleration and the westward bending of Denman’s ice tongue.